NLO electroweak contributions to gluino pair production at hadron colliders

JHEP12(2009)012

(http://iopscience.iop.org/1126-6708/2009/12/012)

Published by IOP Publishing for SISSA

Received: *September 2, 2009*
Accepted: *November 3, 2009*
Published: *December 2, 2009*

JHEP12(2009)012

NLO electroweak contributions to gluino pair production at hadron colliders

E. Mirabella

Max-Planck-Institut für Physik, Werner-Heisenberg-Institut, Föhringer Ring 6, D-80805 München, Germany

E-mail: mirabell@mppmu.mpg.de

Abstract: We calculate the full $\mathcal{O}(\alpha_s^2\alpha)$ corrections to the process of gluino pair production at hadron colliders in the framework of the real MSSM. We show that these contributions can be neglected at the LHC performing a scan over a wide region of the parameter space. The impact of these corrections in the parameter range investigated at the Tevatron is small.

Keywords: Supersymmetric Standard Model, NLO Computations, Hadronic Colliders

ArXiv ePrint: 0908.3318v1

doi:10.1088/1126-6708/2009/12/012

Contents

JHEP12(2009)012

1 Introduction

Despite of its success, the Standard Model (SM) of particle physics is affected by theoretical and phenomenological problems whose solution can be used as a guideline for its extension. In this respect Supersymmetry (SUSY) [1, 2], and in particular the Minimal Supersymmetric extension of the Standard Model (MSSM) [3–5], is one of the most promising scenarios for physics beyond the Standard Model. In SUSY models the breaking of electroweak symmetry is obtained radiatively at a scale which is stabilized by Supersymmetry itself. Moreover, the comparison of MSSM predictions and electroweak precision observables provides an overall fit of data [6, 7] which is at least as good as that obtained using the SM, and even better in the case of specific observables such as $g-2$ of the muon [8, 9].

These features render SUSY an appealing framework, and they can explain the big effort in the hunting for SUSY not only in the past but also in future years. In particular, this search is one of the major goals of the LHC. Experimental studies have shown the possibility of early discovery of SUSY with 1 fb^{-1} of integrated luminosity in the inclusive multijet plus missing E_T channel [10, 11], provided that the masses of squarks and gluinos are not too heavy (e.g. < 2 TeV). Interestingly, the 95 % confidence level area of the

$(m_0, m_{1/2})$ plane of the Constrained MSSM (CMSSM) lies largely in the region that will be investigated with 1 fb^{-1} at 14 TeV [7].

At hadron colliders, colored particles can be searched for most efficiently. This implies that Supersymmetry could be discovered looking at the production of squarks and gluinos. Among the others, the process of gluino pair production,

$$P\ P \to \tilde{g}\ \tilde{g}\ X, \tag{1.1}$$

is one of the most important processes leading to the production of colored SUSY particles. Indeed, its cross section is large, $\mathcal{O}(10$ pb) if the gluino mass is $\mathcal{O}(600$ GeV). Moreover, the gluino plays a key role in characterizing SUSY models. The measure of the spin of a (supposed to be) gluino [12] and the confirmation of its Majorana nature [13–15] would allow not only to distinguish among different beyond Standard Model scenarios, but also among MSSM and others SUSY models involving Dirac gauginos, such as the $N = 1/N = 2$ hybrid scheme [16].

The total cross section for gluino pair production was computed at Born level long time ago [17–20]. NLO SUSY-QCD contributions were computed in ref. [21]. These corrections are positive and large (from 5 to 90%, depending on the masses of the squarks and of the gluino), and they reduce appreciably the factorization scale dependence. They are included into the publicly available code `Prospino` [22]. More recent is the resummation of the QCD Sudakov logarithms at the next-to-leading-logarithmic (NLL) accuracy [23, 24], and the resummation of the leading Coulomb corrections [24]. Their inclusion further stabilizes the prediction against scale variation. The NLL contributions are of the order of $2-8\%$ of the NLO QCD predictions, provided the squark and gluino masses are $\mathcal{O}(1$ TeV). In this mass range the contribution of the Coulomb corrections amounts up to 5%. The computation of NLO electroweak (EW) corrections, of $\mathcal{O}(\alpha_s^2\alpha)$, to the process of hadronic production of a gluino pair is still missing. In this paper, we fill this gap computing the full $\mathcal{O}(\alpha_s^2\alpha)$ corrections to the process (1.1) in the framework of the real MSSM. Our computation is part of an ongoing project aiming to evaluate the tree-level EW and NLO EW contributions to the production of colored SUSY particles at the LHC [25–29].

The plan of the paper is the following. In section 2 we briefly summarize the $\mathcal{O}(\alpha_s^2)$ contributions to the process (1.1). In section 3 we describe the partonic processes contributing at $\mathcal{O}(\alpha_s^2\alpha)$. Numerical results for the electroweak corrections to gluino pair production at the LHC are presented in section 4, while section 5 is devoted to a brief discussion on the numerical value of the electroweak corrections at the Tevatron. Section 6 summarizes our results. A list of Feynman diagrams is collected in the appendix.

2 Gluino pair production in lowest order

The leading order contributions to the process (1.1) are of QCD origin, of $\mathcal{O}(\alpha_s^2)$. At lowest order in the perturbative expansion the differential cross section can be written as follows,

$$d\sigma^{\text{QCD, LO}}_{PP\to\tilde{g}\tilde{g}}(S) = \sum_q \int_{\tau_0}^1 d\tau \frac{dL_{q\overline{q}}}{d\tau}(\tau) d\sigma^{2,0}_{q\overline{q}\to\tilde{g}\tilde{g}}(\tau S) + \int_{\tau_0}^1 d\tau \frac{dL_{gg}}{d\tau}(\tau) d\sigma^{2,0}_{gg\to\tilde{g}\tilde{g}}(\tau S), \tag{2.1}$$

JHEP12(2009)012

with the help of the parton luminosities, defined according to

$$\frac{dL_{ij}}{d\tau}(\tau) = \frac{1}{1+\delta_{ij}} \int_\tau^1 \frac{dx}{x} \left[f_{i|P}(x) f_{j|P}\left(\frac{\tau}{x}\right) + f_{j|P}(x) f_{i|P}\left(\frac{\tau}{x}\right) \right]. \tag{2.2}$$

$f_{i|H}(x)$ is the momentum distribution of the parton i inside the hadron H. The sum runs over the quarks $q = u,\ d,\ c,\ s,\ b$. The lower limit on the integral over τ, $\tau_0 = 4\,m_{\tilde{g}}^2/S$, is related to the threshold for the production of the gluino pair. We use the convention $d\sigma_X^{a,b}$ to denote the cross section for a partonic process X at a given order $\mathcal{O}(\alpha_s^a \alpha^b)$ in the strong and electroweak coupling constants. Therefore, $d\sigma^{2,0}_{q\bar{q}\to\tilde{g}\tilde{g}}$ and $d\sigma^{2,0}_{gg\to\tilde{g}\tilde{g}}$ are the lowest order differential cross sections for the partonic processes

$$q(p_1)\ \overline{q}(p_2) \ \to\ \tilde{g}(k_1)\ \tilde{g}(k_2), \tag{2.3}$$

$$g(p_1)\ g(p_2) \ \to\ \tilde{g}(k_1)\ \tilde{g}(k_2), \tag{2.4}$$

respectively. The cross sections are averaged (summed) over the spins and the colors of the incoming (outgoing) particles. In this analysis we will consider the five light quarks as massless and we approximate the CKM matrix by the unity matrix. We retain the mass of the bottom in the Yukawa couplings, owing to the possible enhancement due to $\tan\beta$. We perform our computation in Feynman gauge.

In lowest order, the partonic cross sections for the processes (2.3) and (2.4) can be obtained from the Feynman diagrams in figure 9 of appendix A. The cross sections can be written as

$$\begin{aligned} d\sigma^{2,0}_{q\bar{q}\to\tilde{g}\tilde{g}} &= \frac{dt}{16\pi s^2} \overline{\sum} \left| \mathcal{M}^{1,0}_{q\bar{q}\to\tilde{g}\tilde{g}} \right|^2, \\ d\sigma^{2,0}_{gg\to\tilde{g}\tilde{g}} &= \frac{dt}{16\pi s^2} \overline{\sum} \left| \mathcal{M}^{1,0}_{gg\to\tilde{g}\tilde{g}} \right|^2, \end{aligned} \tag{2.5}$$

where $\mathcal{M}^{1,0}_X$ is the tree-level contribution to the amplitude of the process X. The squared amplitudes averaged (summed) over the spins and the colors of the initial (final) particles read [17–21]

$$\begin{aligned} \overline{\sum} \left| \mathcal{M}^{1,0}_{q\bar{q}\to\tilde{g}\tilde{g}} \right|^2 &= \frac{8}{27}\,\alpha_s^2\,\pi^2 \left\{ \frac{72}{s^2}\left(2m_{\tilde{g}}^2 s + t_{\tilde{g}}^2 + u_{\tilde{g}}^2\right) + 4m_{\tilde{g}}^2 s \left(\frac{1}{u_{\tilde{q},1} t_{\tilde{q},1}} + \frac{1}{u_{\tilde{q},2} t_{\tilde{q},2}} \right) \right. \\ &\quad + \frac{36(m_{\tilde{g}}^2 s + t_{\tilde{g}}^2)}{s} \left(\frac{1}{t_{\tilde{q},1}} + \frac{1}{t_{\tilde{q},2}} \right) + 16 t_{\tilde{g}}^2 \left(\frac{1}{t_{\tilde{q},1}^2} + \frac{1}{t_{\tilde{q},2}^2} \right) \\ &\quad \left. + \frac{36(m_{\tilde{g}}^2 s + u_{\tilde{g}}^2)}{s} \left(\frac{1}{u_{\tilde{q},1}} + \frac{1}{u_{\tilde{q},2}} \right) + 16 u_{\tilde{g}}^2 \left(\frac{1}{u_{\tilde{q},1}^2} + \frac{1}{u_{\tilde{q},2}^2} \right) \right\}, \\ \overline{\sum} \left| \mathcal{M}^{1,0}_{gg\to\tilde{g}\tilde{g}} \right|^2 &= 18\,\alpha_s^2\,\pi^2 \left\{ \left(1 - \frac{t_{\tilde{g}} u_{\tilde{g}}}{s^2}\right) \left[\frac{s^2}{t_{\tilde{g}} u_{\tilde{g}}} - 2 + 4\frac{m_{\tilde{g}}^2 s}{t_{\tilde{g}} u_{\tilde{g}}} \left(1 - \frac{m_{\tilde{g}}^2 s}{t_{\tilde{g}} u_{\tilde{g}}}\right) \right] \right\}. \end{aligned} \tag{2.6}$$

JHEP12(2009)012

A factor 1/2 has been taken into account because of the identical particles in the final states. The Mandelstam variables are defined as

$$\begin{aligned} s &= (p_1 + p_2)^2, & & & \\ t &= (p_2 - k_2)^2, & t_{\tilde{q},a} &= t - m^2_{\tilde{q},a}, & t_{\tilde{g}} &= t - m^2_{\tilde{g}}, \\ u &= (p_1 - k_2)^2, & u_{\tilde{q},a} &= u - m^2_{\tilde{q},a}, & u_{\tilde{g}} &= u - m^2_{\tilde{g}}, \end{aligned} \tag{2.7}$$

and $u = 2m^2_{\tilde{g}} - s - t$.

3 $\mathcal{O}(\alpha_s^2\alpha)$ corrections to the hadronic process

Gluinos do not interact weakly, thus a pair of gluinos is neither produced at $\mathcal{O}(\alpha^2)$, from $q\bar{q}$ initial states, nor at $\mathcal{O}(\alpha_s\alpha)$ via photon-induced processes. Therefore, in contrast to squark–anti-squark [25, 27, 28] and squark-gluino [29] production, EW contributions enter only at NLO, and they are at least of $\mathcal{O}(\alpha_s^2\alpha)$. The NLO EW contributions to the hadronic differential cross section reads as follows,

$$\begin{aligned} d\sigma^{\text{EW NLO}}_{PP\to\tilde{g}\tilde{g}X}(S) = \sum_q \Bigg\{ \int_{\tau_0}^1 d\tau \Bigg[\frac{dL_{q\bar{q}}}{d\tau}(\tau) \Big(d\sigma^{2,1}_{q\bar{q}\to\tilde{g}\tilde{g}}(\tau S) + d\sigma^{2,1}_{q\bar{q}\to\tilde{g}\tilde{g}\gamma}(\tau S) \Big) \\ + \frac{dL_{q\gamma}}{d\tau}(\tau) d\sigma^{2,1}_{q\gamma\to\tilde{g}\tilde{g}q}(\tau S) + \frac{dL_{\gamma\bar{q}}}{d\tau}(\tau) d\sigma^{2,1}_{\gamma\bar{q}\to\tilde{g}\tilde{g}\bar{q}}(\tau S) \Bigg] \Bigg\}. \end{aligned} \tag{3.1}$$

The $q\gamma$ and $\gamma\bar{q}$ luminosities entering (3.1) are built according to eq. (2.2). Besides the virtual corrections and the real photon radiation processes at $\mathcal{O}(\alpha_s^2\alpha)$, we consider the photon-induced processes leading to the production of a gluino pair together with an (anti-)quark. Diagrams and amplitudes are generated with `FeynArts` [30, 31]. The reduction of the one-loop integrals is performed with the help of `FormCalc` [32, 33], while the scalar one-loop integrals are numerically evaluated using `LoopTools`. Infrared (IR) and collinear singularities are treated using mass regularization, i.e. giving a small mass to the photon and to the five light quarks.

3.1 $q\bar{q}$ annihilation with electroweak loops

The first class of corrections entering eq. (3.1) are the electroweak one-loop corrections to the processes (2.3), yielding the following partonic cross section,

$$d\sigma^{2,1}_{q\bar{q}\to\tilde{g}\tilde{g}} = \frac{dt}{16\pi s^2} \overline{\sum} 2\,\mathfrak{Re}\left\{ \mathcal{M}^{1,0*}_{q\bar{q}\to\tilde{g}\tilde{g}} \mathcal{M}^{1,1}_{q\bar{q}\to\tilde{g}\tilde{g}} \right\}. \tag{3.2}$$

$\mathcal{M}^{1,1}_{q\bar{q}\to\tilde{g}\tilde{g}}$ is the one-loop electroweak contribution to the amplitude of the quark–anti-quark annihilation process. The diagrams responsible for this contribution are displayed in figure 12 of appendix A.

We treat UV divergences using dimensional reduction. In order to cure the UV divergences we have to renormalize the quark and the squark sector at $\mathcal{O}(\alpha)$. Renormalization of mass and wavefunction of the quarks and squarks belonging to the first two generations,

JHEP12(2009)012

of $\tan\beta$ and of the mass of the W boson, has been performed according to the procedure described in ref. [28]. The renormalization of mass and wavefunction of the bottom and top quarks and squarks has been widely studied [34–38], and several renormalization schemes have been proposed. Each of these schemes has its own virtues and drawbacks, we perform our computation using two different renormalization schemes. The first (second) scheme, referred in the following as Rs1 (Rs2), is the "m_b OS" ("m_b $\overline{\rm DR}$") scheme defined in ref. [38]. The renormalization of the stop-sbottom sector at $\mathcal{O}(\alpha)$ within the Rs2 scheme requires the renormalization of the supersymmetric Higgs parameter μ. This parameters has been defined in the $\overline{\rm DR}$ scheme.

In the case of $b\bar{b} \to \tilde{g}\tilde{g}$ we keep the mass of the b-quark that appears in the couplings. In this case, the last twelve diagrams in figure 12 of the appendix A have to be considered as well. It is well known [39–44] that, in the large $\tan\beta$ regime, the tree-level relation between the bottom mass m_b and the bottom Yukawa couplings y_b receives radiative corrections that can be strongly enhanced and have to be resummed. Power counting in $\alpha_s \tan\beta$ shows that the leading $\tan\beta$ enhanced contributions, of $\mathcal{O}(\alpha_s^n \tan^n\beta)$, can be accounted for by means of the substitution

$$m_b^{\rm Rs} \to \overline{m}_b^{\rm Rs} = \frac{m_b^{\rm Rs}}{1+\Delta_b} \tag{3.3}$$

in the relation between m_b and y_b. $m_b^{\rm Rs}$ is the bottom mass in a given renormalization scheme, Rs. Δ_b is defined as

$$\Delta_b = \frac{2\alpha_s}{3\pi}\frac{m_{\tilde{g}}\,\mu\,\tan\beta}{(m^2_{\tilde{b},1}-m^2_{\tilde{b},2})(m^2_{\tilde{b},2}-m^2_{\tilde{g}})(m^2_{\tilde{b},1}-m^2_{\tilde{g}})}\left[m^2_{\tilde{b},1}m^2_{\tilde{b},2}\ln\left(\frac{m^2_{\tilde{b},1}}{m^2_{\tilde{b},2}}\right)\right.$$
$$\left. + m^2_{\tilde{b},2}m^2_{\tilde{g}}\ln\left(\frac{m^2_{\tilde{b},2}}{m^2_{\tilde{g}}}\right) + m^2_{\tilde{g}}m^2_{\tilde{b},1}\ln\left(\frac{m^2_{\tilde{g}}}{m^2_{\tilde{b},1}}\right)\right]. \tag{3.4}$$

Concerning the Higgs sector, the $b-\bar{b}-h_u^0$ coupling is dynamically generated at $\mathcal{O}(\alpha_s)$. This coupling can be enhanced if $\tan\beta$ is large and it is worth to include such effects modifying the $b-\bar{b}$–Higgs Yukawa couplings. In particular, the effective Lagrangian that correctly takes into account these dynamically generated extra-couplings is

$$\mathcal{L}^{\rm eff.}_{\rm Higgs} = \frac{\overline{m}_b^{\rm Rs}}{v}\left[\tan\beta\left(1-\frac{\Delta_b}{\tan^2\beta}\right)A^0\bar{b}i\gamma^5 b + \frac{\sin\alpha}{\cos\beta}\left(1-\frac{\Delta_b}{\tan\alpha\tan\beta}\right)h^0\bar{b}b\right.$$
$$\left. -\frac{\cos\alpha}{\cos\beta}\left(1+\frac{\Delta_b\tan\alpha}{\tan\beta}\right)H^0\bar{b}b\right]. \tag{3.5}$$

3.2 $q\bar{q}$ annihilation with real photon emission

IR singularities in the virtual corrections are cancelled when the tree-level contribution of the partonic process of real photon radiation,

$$q(p_1)\;\overline{q}(p_2) \to\; \tilde{g}(k_1)\;\tilde{g}(k_2)\;\gamma(k_3), \tag{3.6}$$

is included. This contribution can be computed using the Feynman diagrams depicted in figure 10 of appendix A. The integral over the phase space is IR divergent when $k_3 \to 0$,

JHEP12(2009)012

while collinear singularities appear whenever $k_3 \cdot p_i \to 0$. IR and collinear divergences appearing in the phase space integration are regularized using both, phase space slicing [45–47] and dipole subtraction [48, 49]. The two methods are in good numerical agreement, as found also in the case of squark-anti–squark production [28]. As already mentioned, IR singularities cancel when the real radiation processes and the virtual contributions are added together, as in eq. (3.1). Collinear singularities remain and have to be absorbed via the factorization of the parton distribution functions (PDFs), c.f. section 3.4.

3.3 $q\gamma$ and $\gamma\bar{q}$ fusion

The last class of $\mathcal{O}(\alpha_s^2\alpha)$ contributions to the process (1.1) are the tree-level contributions of the partonic processes

$$q(p_1)\,\gamma(p_2) \to \tilde{g}(k_1)\,\tilde{g}(k_2)\,q(k_3), \tag{3.7}$$
$$\gamma(p_1)\,\overline{q}(p_2) \to \tilde{g}(k_1)\,\tilde{g}(k_2)\,\overline{q}(k_3). \tag{3.8}$$

These contributions can be computed from the Feynman diagrams depicted in figure 11 of appendix A.

Note that, if $m_{\tilde{q}} > m_{\tilde{g}}$, the quark in the final state can be the decay product of an on-shell squark. If this is the case the last four diagrams depicted in figure 11 become singular. The related poles have to be regularized inserting the width of the on-shell squarks into the corresponding propagator. Furthermore, the contribution obtained squaring the resonant diagrams has to be subtracted since it arises from the production and the subsequent decay of an (anti-)squark through (anti-)quark–photon fusion,

$$\begin{aligned} q\,\gamma &\to \tilde{g}\tilde{q} \quad \text{and} \quad \tilde{q} \to \tilde{g}\,q, \\ \gamma\,\bar{q} &\to \tilde{g}\tilde{q}^* \quad \text{and} \quad \tilde{q}^* \to \tilde{g}\,\bar{q}. \end{aligned} \tag{3.9}$$

According to refs. [21, 29], the extraction of the Breit-Wigner pole contribution has been performed in the narrow width approximation.

Collinear singularities arising from initial state emission are again absorbed into the PDFs. These singularities are regularized using both, phase space slicing and dipole subtraction. The formulae needed can be found in ref. [45] and in refs. [49, 50], respectively. The results obtained using the two methods agree within the integration uncertainty.

The contribution of this channel is expected to be small owing to the suppression of the photon PDF inside the proton. Indeed, the photon PDF is intrinsically suppressed with respect to the valence quark PDF by a factor α, since this PDF is originated from the emission of a photon from a (anti-)quark. In the SUSY scenarios we consider, the contribution of this partonic process amounts up to few percent of the whole $\mathcal{O}(\alpha_s^2\alpha)$ correction.

3.4 Factorization of initial collinear singularities

As already mentioned, the universal logarithmic divergences related to the collinear splittings

$$q \to q\,\gamma, \quad \bar{q} \to \bar{q}\,\gamma, \quad \gamma \to q\,\bar{q},$$

JHEP12(2009)012

are absorbed into the definition of the PDFs via mass factorization. We factorize the (anti-)quark PDFs at $\mathcal{O}(\alpha)$ in the DIS scheme. The effect of this factorization is to add the following term into eq. (3.1),

$$d\sigma^{\text{Fact.}}_{PP\to\tilde{g}\tilde{g}X}(S) = \int_{\tau_0}^1 d\tau \sum_q \left\{ \left[-\frac{\alpha}{\pi} e_q^2 \frac{dL_{q\overline{q}}}{d\tau}(\tau) \int_{z_0}^1 dz \left[\mathcal{H}_q^{(1)}\right]_+ d\sigma^{2,0}_{q\overline{q}\to\tilde{g}\tilde{g}}(z\tau S) \right.\right.$$
$$\left.\left. -\frac{3\alpha}{2\pi} e_q^2 \left(\frac{dL_{q\gamma}}{d\tau}(\tau) + \frac{dL_{\gamma\overline{q}}}{d\tau}(\tau) \right) \int_{z_0}^1 dz \left(\mathcal{H}_q^{(2)}\right) d\sigma^{2,0}_{q\overline{q}\to\tilde{g}\tilde{g}}(z\tau S) \right] \right\}. \tag{3.10}$$

The functions $\mathcal{H}_q^{(1)}$ and $\mathcal{H}_q^{(2)}$ read as follows,

$$\mathcal{H}_q^{(1)} = P_{qq}(z) \left[\ln\left(\frac{\mu_F^2}{m_q^2} \frac{1}{z(1-z)} \right) - 1 \right] - \frac{3}{2} \frac{1}{1-z} + 2z + 3,$$
$$\mathcal{H}_q^{(2)} = P_{q\gamma}(z) \ln\left(\frac{\mu_F^2}{m_q^2} \frac{1-z}{z} \right) - 1 + 8z - 8z^2, \tag{3.11}$$

where the splitting functions are

$$P_{qq}(z) = \frac{1+z^2}{1-z}, \qquad P_{q\gamma}(z) = z^2 + (1-z)^2.$$

z_0 is defined as $z_0 = 4m_{\tilde{g}}/(\tau S)$, while e_q is the charge of the quark q expressed in units of the positron charge. The $[\cdots]_+$ distribution is defined as

$$\int_a^1 dx\, [f(x)]_+ g(x) = \int_a^1 dx\, f(x)\big[g(x) - g(1)\big] - g(1) \int_0^a dx\, f(x). \tag{3.12}$$

In the actual computation, we use the MRST2004qed parton distribution functions at NLO QED and NLO QCD [51]. This fit takes into account QED-effects into the DGLAP evolution equations and the parametrization of the PDF at the initial scale. MRST2004qed PDFs are defined at NLO QCD within the $\overline{\text{MS}}$ mass factorization scheme. As discussed in ref. [50], the DIS scheme is used for the factorization of the $\mathcal{O}(\alpha)$ corrections.

In our computation we set the renormalization scale, μ_R, equal to the factorization scale, μ_F, and to the gluino mass, i.e. $\mu_R = \mu_F = m_{\tilde{g}}$.

4 Numerical results, LHC

For our numerical discussion we use the Standard Model parameters quoted in ref. [52]. The value of the bottom mass in the $\overline{\text{DR}}$ scheme is computed according to ref. [38]. We choose two different SUSY scenarios. The first scenario is the SPS1a′ suggested by the Supersymmetry Parameters Analyses (SPA) [53] project. The second one, called SPS2, belongs to the set of Snowmass Points and Slopes, introduced in ref. [54]. We obtain the parameters of the two scenarios with the help of the program `SPheno` [55], starting from the input parameters shown in table 1. The low-energy input parameters for these scenarios are collected in table 5 of appendix B.

JHEP12(2009)012

parameter	SPS1a′	SPS2
$m_{1/2}$	250 GeV	300 GeV
m_0	70 GeV	1450 GeV
A_0	−300 GeV	0
sign(μ)	” + ”	” + ”
$\tan\beta(M_Z)$	10.37	10

Table 1. MSSM input parameters for the computation of the spectrum of the two scenarios considered. $m_{1/2}$, m_0 and A_0 are defined at the GUT scale.

point	$\sigma^{\text{QCD, LO}}$	$\sigma^{\text{QCD, LO}} + \sigma^{\text{EW, NLO}}$	δ	$\frac{1}{\sqrt{L\cdot\sigma^{\text{QCD, LO}}}}$
SPS1a′	6.1865(6) pb	6.1822(6) pb	−0.07%	0.13%
SPS2	1.2127(1) pb	1.2089(1) pb	−0.31%	0.29%

Table 2. Total hadronic cross section for gluino pair production at the LHC ($\sqrt{S} = 14\,\text{TeV}$). In the second (third) column we show the $\mathcal{O}(\alpha_s^2)$ ($\mathcal{O}(\alpha_s^2 + \alpha_s^2\alpha)$) contribution for the points SPS1a′ and SPS2. In the fourth column the electroweak corrections relative to the LO + NLO EW result are given. The last column shows an estimate of the statistical error affecting the measurement of the total cross section for an integrated luminosity $L = 100$ fb^{-1}. The numbers in parentheses are the numerical uncertainties on the last digit.

4.1 Dependence on the SUSY scenario

We compute the total hadronic cross section, the results are collected in table 2. The second column shows the lowest order results. The third column shows the sum of the lowest order and of the $\mathcal{O}(\alpha_s^2\alpha)$ contributions. In the fourth column the contribution of the $\mathcal{O}(\alpha_s^2\alpha)$ corrections relative to the total result is given, i.e. δ is defined as

$$\delta \equiv \frac{\sigma^{\text{EW, NLO}}}{\sigma^{\text{QCD, LO}} + \sigma^{\text{EW, NLO}}}.$$

In the last entry we give an estimate of the statistical error affecting the measurement of the total cross section based on an integrated luminosity of $L = 100$ fb^{-1} [56]. We do not distinguish the results in the different renormalization schemes since they agree within the integration error. A priori this is not guaranteed. Indeed the Rs1 scheme turns out to be unreliable in the scenarios we are considering. In this scheme, the finite part of the renormalization constant of the trilinear coupling, δA_b^{fin}, is comparable with the value of the trilinear coupling A_b itself, i.e. $\delta A_b^{\text{fin}}/A_b \sim 1$, and the perturbative expansion is spoiled. However, the difference among the renormalization schemes is as small as few percent of the tree-level $b\bar{b}$ annihilation channel cross section. The latter contributions amount up to several fb, therefore the variation of the results in table 2 is within the integration error.

As one can see, in the case of the point SPS1a′ the electroweak corrections are much smaller than the statistical uncertainty and so they are not relevant. In the case of the point SPS2, the $\mathcal{O}(\alpha_s^2\alpha)$ corrections are of the same order of the statistical error but they are smaller than the theoretical systematic uncertainties such as the uncertainty on the

JHEP12(2009)012

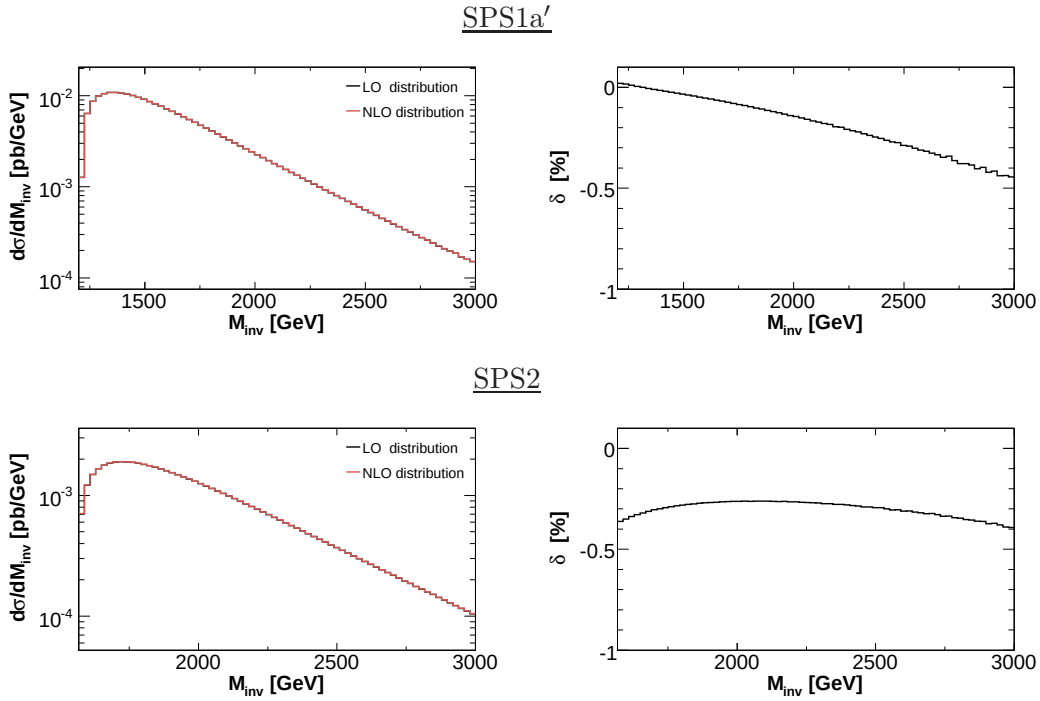

Figure 1. Invariant mass distribution for gluino pair production at the LHC. In the left panels we show the LO (black line) and the LO + NLO EW (red line) distribution. The two lines are indistinguishable, owing to the smallness of the EW contributions. In the right panels the electroweak correction relative to the total result is shown.

PDF parametrization ($\lesssim 10\%$) [21] and the factorization scale dependence (from 3 to 5% if $m_{\tilde{g}} \leq 1\,\text{TeV}$) [24].

The invariant mass distribution of the two gluinos is shown in figure 1. The EW corrections are small, their absolute value being at most of the order of 0.4% of the total contribution. Moreover, these corrections do not distort the shape of the distribution.

In figure 2 we consider the distribution of the largest transverse momentum of the two gluinos, for brevity we will refer to this observable as "transverse momentum distribution". The $\mathcal{O}(\alpha_s^2\alpha)$ corrections are rather small, the absolute value of their contribution relative to the total result is at most 1%, reaching this value in the high p_T region, for $p_T \gtrsim 1500\,\text{GeV}$.

4.2 Dependence on the MSSM parameters

In this subsection we investigate the size of the $\mathcal{O}(\alpha_s^2\alpha)$ corrections to gluino pair production in a more systematic way, performing a scan over the parameter space of the MSSM. The parameters involved in the scan are the independent parameters in the second renormalization scheme. We suppose that all the sfermionic soft mass parameters are equal and we indicate their value in the Rs2 scheme as M_{Susy}. The physical masses of the sfermions can be obtained from M_{Susy} diagonalizing the mass matrices. Moreover, we consider the surfaces of the parameter space characterized by $A_t = A_\tau$. With these assumptions there

JHEP12(2009)012

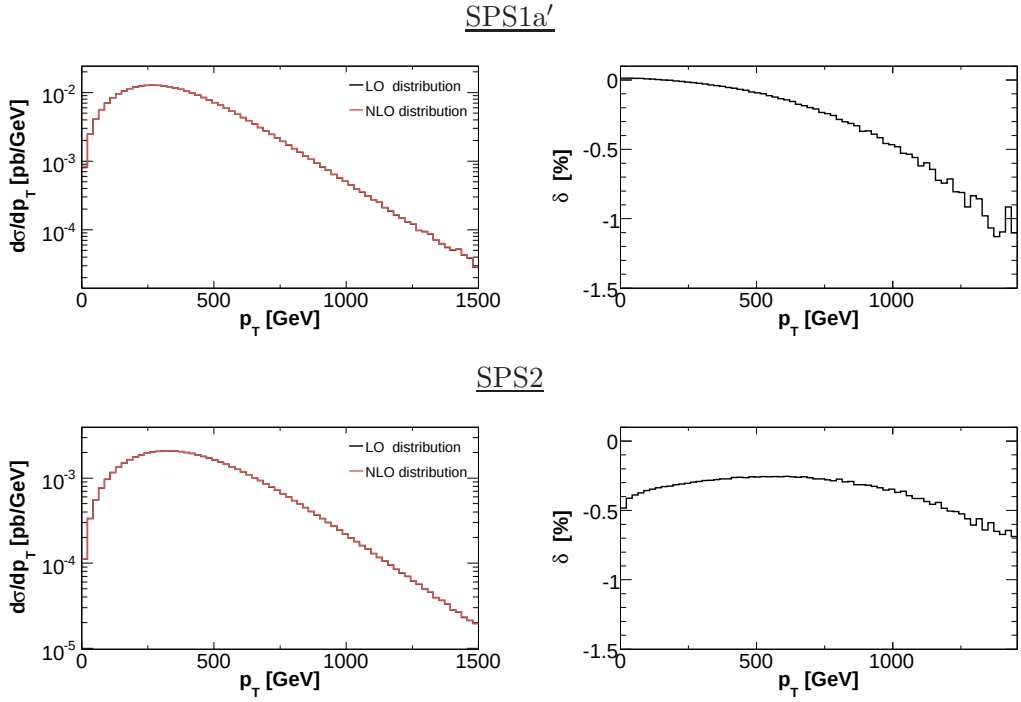

Figure 2. Same as figure 1, but considering the transverse momentum distribution.

are eight independent parameters involved in the scan, namely,

$$M_{\rm Susy}, \quad m_{\tilde{g}}, \quad \mu, \quad M_2, \quad A_t, \quad A_b, \quad \tan\beta, \quad m_{A^0}.$$

The subregions of the parameter space are chosen imposing the exclusion limits arising from SUSY searches at LEP [57] and at the Tevatron [58], and the bound on the mass of the light Higgs boson. The physical mass of the light Higgs boson has been computed using `FeynHiggs 2.5.1` [59–61]. Moreover, each point in the selected regions fulfills the condition $|\Delta\rho| \leq 0.025$, $\Delta\rho$ being the dominant SUSY corrections to the electroweak ρ parameter, corrections arising from top and bottom squarks contributions.

We perform four different scans. In each scan we select two parameters and we study the dependence of the quantity Δ,

$$\Delta \equiv \frac{\sigma^{\rm EW,\ NLO}}{\sigma^{\rm QCD,\ LO} + \sigma^{\rm EW,\ NLO}} \cdot 100.$$

We repeat each of these scans for different values of another pair of parameters, while the remaining four are fixed to their SPS1a′ values. Here there is a brief discussion on the results of these scans.

Scan over A_t and A_b. The results of this scan are displayed in figure 3. As expected, Δ is quite independent on the parameter A_t which enters in the virtual correction of the process $b\bar{b} \to \tilde{g}\tilde{g}$ and in the definition of the mass of the top squarks. This feature is more evident for large $\tan\beta$ values. Δ varies only by an amount of the order of few percent for

JHEP12(2009)012

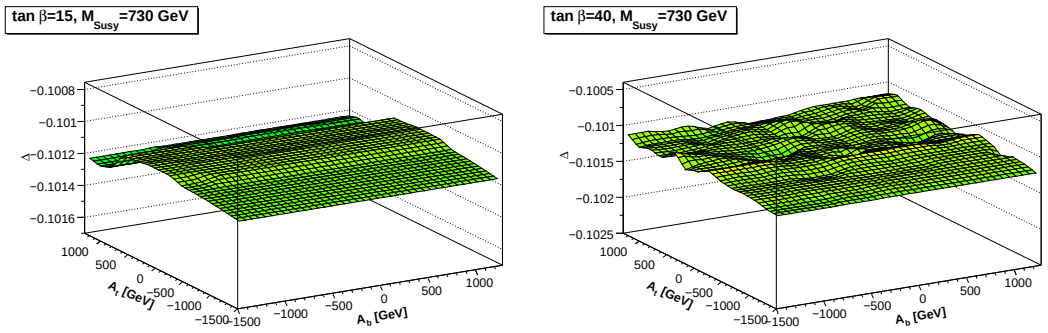

Figure 3. $\Delta = \sigma^{\mathrm{EW,\,NLO}}/(\,\sigma^{\mathrm{QCD,\,LO}} + \sigma^{\mathrm{EW,\,NLO}}\,) \cdot 100$ as a function of A_t and A_b for different values of $\tan\beta$ and M_{Susy}. The other parameters are fixed to their SPS1a′ values.

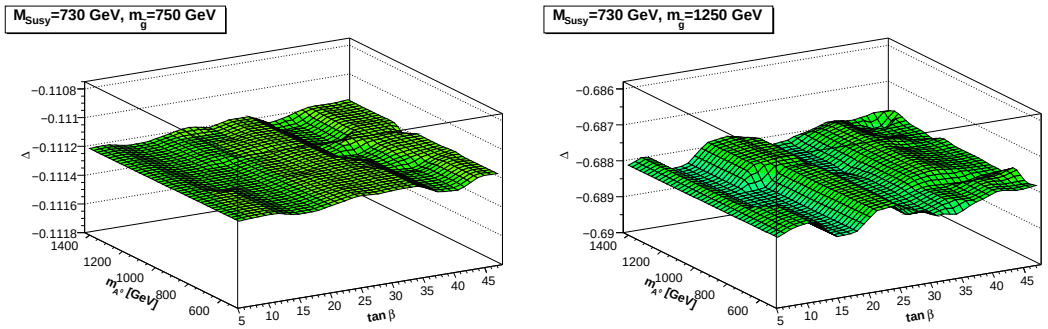

Figure 4. $\Delta = \sigma^{\mathrm{EW,\,NLO}}/(\,\sigma^{\mathrm{QCD,\,LO}} + \sigma^{\mathrm{EW,\,NLO}}\,) \cdot 100$ as a function of $\tan\beta$ and m_{A^0} for different values of $m_{\tilde{g}}$ and M_{Susy}. The other parameters are fixed to their SPS1a′ values.

a variation of A_b and A_t over a quite broad range (from -1500 to $1500\,\mathrm{GeV}$). Note that in the whole subregion considered the absolute value of Δ is of $\mathcal{O}(0.1)$.

Scan over $\tan\beta$ and m_{A^0}. As can be inferred from figure 4, the dependence of Δ on $(\tan\beta, m_{A^0})$ strongly varies for different values of $m_{\tilde{g}}$ and M_{Susy}. As a general result the overall dependence is mild for each value of $(m_{\tilde{g}}, M_{\mathrm{Susy}})$. In all cases the value of $|\Delta|$ is at most of the order of 0.7.

Scan over μ and M_2. As displayed in figure 5, Δ is almost independent on μ for each value of the pair $(m_{\tilde{g}}, M_{\mathrm{Susy}})$ while the dependence on M_2 is more important and particularly pronounced when $m_{\tilde{g}} = 1250\,\mathrm{GeV}$ and $M_{\mathrm{Susy}} = 730\,\mathrm{GeV}$. In the case of the last three plots the value of Δ is of order -0.3 to -0.1, while in the first plot, characterized by $m_{\tilde{g}} \sim 2{\cdot}M_{\mathrm{Susy}}$, the value of Δ is enhanced for small values of M_2 reaching the value of -0.65.

Notice that the mass of the lightest neutralino and chargino is almost independent on the value of μ but varies strongly as M_2 varies, growing as the value of this parameter grows. So this enhancement occurs when charginos/neutralinos are much lighter than the gluino.

Scan over M_{Susy} and $m_{\tilde{g}}$. In this scan we investigate the dependence of Δ on $m_{\tilde{g}}$ and M_{Susy}, which is expected to be the most important because of the dependence of the lowest order cross section on these parameters. We consider the variation of Δ as a function of

JHEP12(2009)012

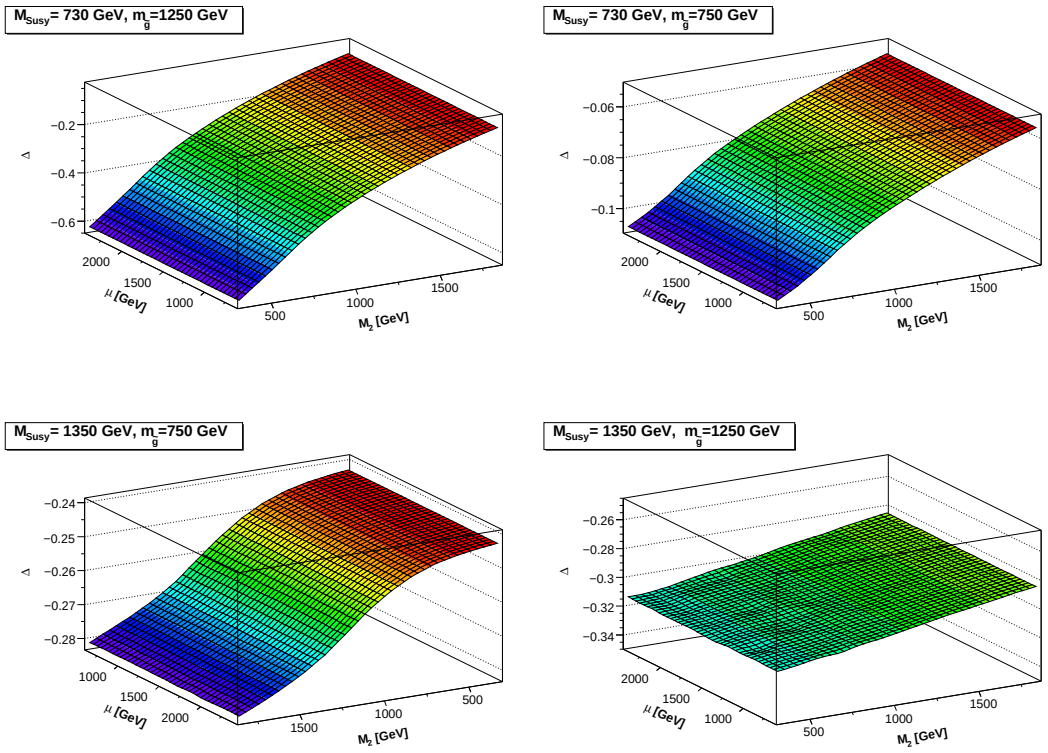

Figure 5. $\Delta = \sigma^{\mathrm{EW,\,NLO}}/(\,\sigma^{\mathrm{QCD,\,LO}}+\sigma^{\mathrm{EW,\,NLO}}\,)\cdot 100$ as a function of μ and M_2 for different values of $m_{\tilde{g}}$ and M_{Susy}. The other parameters are fixed to their SPS1a′ values.

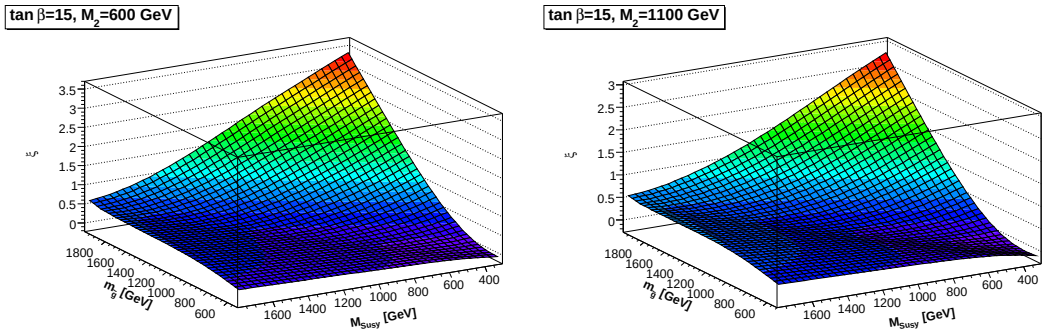

Figure 6. $\xi \equiv -\Delta = -\sigma^{\mathrm{EW,\,NLO}}/(\,\sigma^{\mathrm{QCD,\,LO}}+\sigma^{\mathrm{EW,\,NLO}}\,)\cdot 100$ as a function of M_{Susy} and $m_{\tilde{g}}$ for different values of M_2 and $\tan\beta$. The other parameters are fixed to their SPS1a′ values.

$(m_{\tilde{g}}, M_{\mathrm{Susy}})$ for different values of M_2 and $\tan\beta$, see figure 6. Note that we plot $\xi \equiv -\Delta$ instead of Δ. As a general feature ξ increases as $m_{\tilde{g}}$ increases and as M_{Susy} decreases. The behaviour of ξ as a function of M_{Susy} and $m_{\tilde{g}}$ is affected by the value of M_2 being enhanced for smaller values of this parameter. In particular $\xi \sim 3$ in the region $m_{\tilde{g}} \geq 1600\,\mathrm{GeV}$, $M_{\mathrm{Susy}} \leq 500\,\mathrm{GeV}$.

The enhancement of the EW corrections is related to the increasing importance of

JHEP12(2009)012

parameter	TP1	TP2
$m_{1/2}$	200 GeV	120 GeV
m_0	130 GeV	500 GeV
A_0	0	0
sign(μ)	" $-$ "	" $-$ "
$\tan\beta(M_Z)$	3	3

Table 3. MSSM input parameters for the computation of the spectrum of the scenarios TP1 and TP2.

the $q\bar{q}$ annihilation channel when the production threshold becomes higher. Indeed, the minimal value of the parton's momentum fraction rises as the gluino mass rises. Since the relative importance of the (anti-)quark PDF increases as the momentum fraction of the (anti-)quark increases, the EW corrections grow as the mass of the gluino grows. The relative importance of the EW contributions is more pronounced when $M_{\rm Susy}$ is small owing to the presence of tree-level diagrams with squarks exchanged in the t and u channel, c.f. figure 9, which are enhanced when the squark masses decrease.

5 Numerical results, Tevatron

The EW contributions to gluino pair production are expected to be more important at the Tevatron than at the LHC, owing to the enhancement of the quark–anti-quark annihilation channels with respect to the gluon fusion channel. Therefore, it is worth to estimate the impact of the EW contributions to gluino pair production at the Tevatron, i.e. to the process

$$P\,\overline{P} \to \tilde{g}\,\tilde{g}\,X. \tag{5.1}$$

The previous analysis can be easily extended to (5.1), provided that the definition of the luminosity, eq. (2.2), is replaced by

$$\frac{dL_{ij}}{d\tau}(\tau) = \frac{1}{1+\delta_{ij}} \int_\tau^1 \frac{dx}{x}\left[f_{i|P}(x) f_{j|\overline{P}}\left(\frac{\tau}{x}\right) + f_{j|P}\left(\frac{\tau}{x}\right) f_{i|\overline{P}}(x)\right]. \tag{5.2}$$

For numerical evaluation, we focus on two different points of the MSSM parameter space, referred to as TP1 and TP2 respectively. These points belong to the region of the parameter space of the MSSM used in the data analysis made by CDF and D0 collaborations [62–64]. We obtain the parameters in these scenarios with the help of `SPheno`, starting from the input parameters at the GUT scale described in table 3. These points are compatible with the experimental limits set by the analysis made by the D0 collaboration [64]. In particular, the first one corresponds to a scenario in which the gluino is heavier than the squarks ($m_{\tilde{g}} \sim 500\,\text{GeV}$, $m_{\tilde{q}\neq\tilde{t}} \sim 460\,\text{GeV}$), while the second one describes a scenario characterized by a light gluino ($m_{\tilde{g}} \sim 340\,\text{GeV}$, and $m_{\tilde{q}\neq\tilde{t}} \sim 550\,\text{GeV}$). The low-energy input parameters for the scenarios TP1 and TP2 are listed in table 5 of appendix B.

In table 4 we show the total hadronic cross section in the two points considered. We

point	$\sigma^{\text{QCD, LO}}$	$\sigma^{\text{QCD, LO}} + \sigma^{\text{EW, NLO}}$	δ	$\frac{1}{\sqrt{L \cdot \sigma^{\text{QCD, LO}}}}$
TP1	0.16714(1) fb	0.16691(1) fb	−0.14%	61 %
TP2	0.048864(3) pb	0.048256(4) pb	−1.26%	3.6 %

Table 4. Same as table 2, but considering gluino pair production at the Tevatron, i.e. the process $P\overline{P} \to \tilde{g}\tilde{g}X$ at $\sqrt{S} = 1.96\,\text{TeV}$, and different SUSY scenarios. The last column shows an estimate of the statistical error affecting the measurement of the total cross section based on an integrated luminosity $L = 2 \times 8\ \text{fb}^{-1}$.

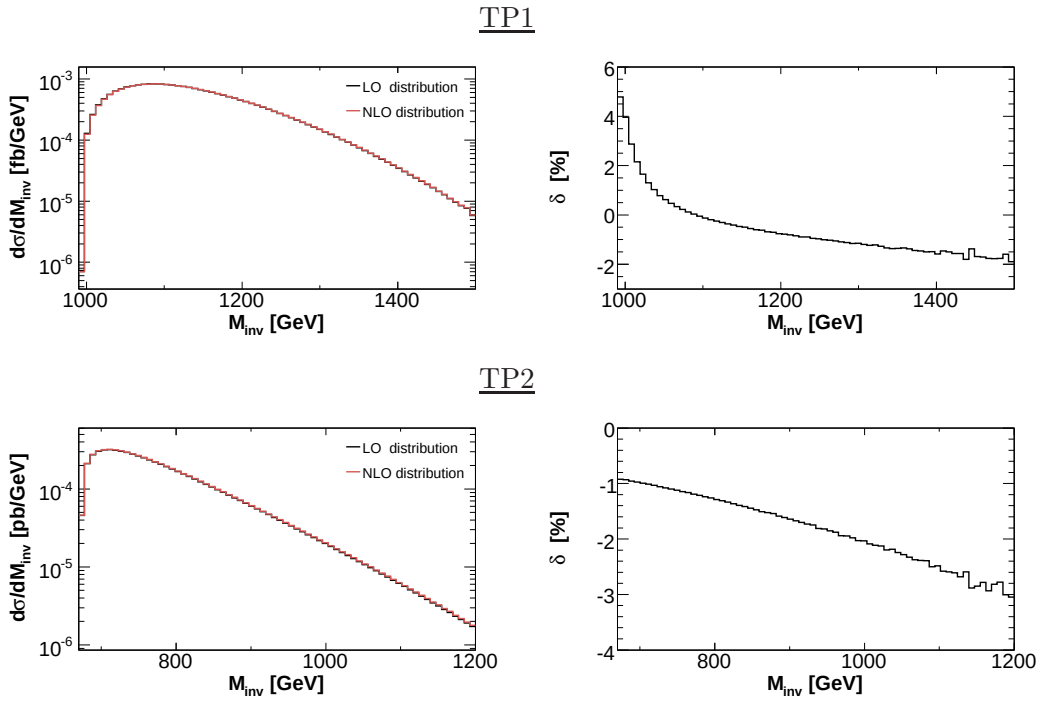

Figure 7. Invariant mass distribution of the two gluinos produced at the Tevatron via the process $P\overline{P} \to \tilde{g}\tilde{g}X$. In the left panels we show the LO and the EW+NLO EW contribution, while the electroweak corrections relative to the total result are shown in the right panels.

use the same notation as in table 2. In the case of the point TP1, the size of the electroweak corrections is so small that they will not be visible at the expected final integrated luminosity $L = 2 \times 8\ \text{fb}^{-1}$. In the case of the point TP2 we obtain a relative statistical error of order 4% which is three times bigger than the size of the electroweak contributions. Moreover it is worth to notice that the systematic uncertainties affecting SUSY searches at the Tevatron are typically greater than 1%. For instance, ref. [64] claims that the μ_F dependence of the total cross section gives an error from 15 to 20%.

The invariant mass distribution for the two points is shown in figure 7. In both cases the $\mathcal{O}(\alpha_s^2\alpha)$ corrections are small compared to the lowest order results and do not change the shape of the distribution. In particular, in the case of the point TP1 (TP2) EW corrections relative to the total contribution are of the order of −2 to 5% (−3 to −1%).

JHEP12(2009)012

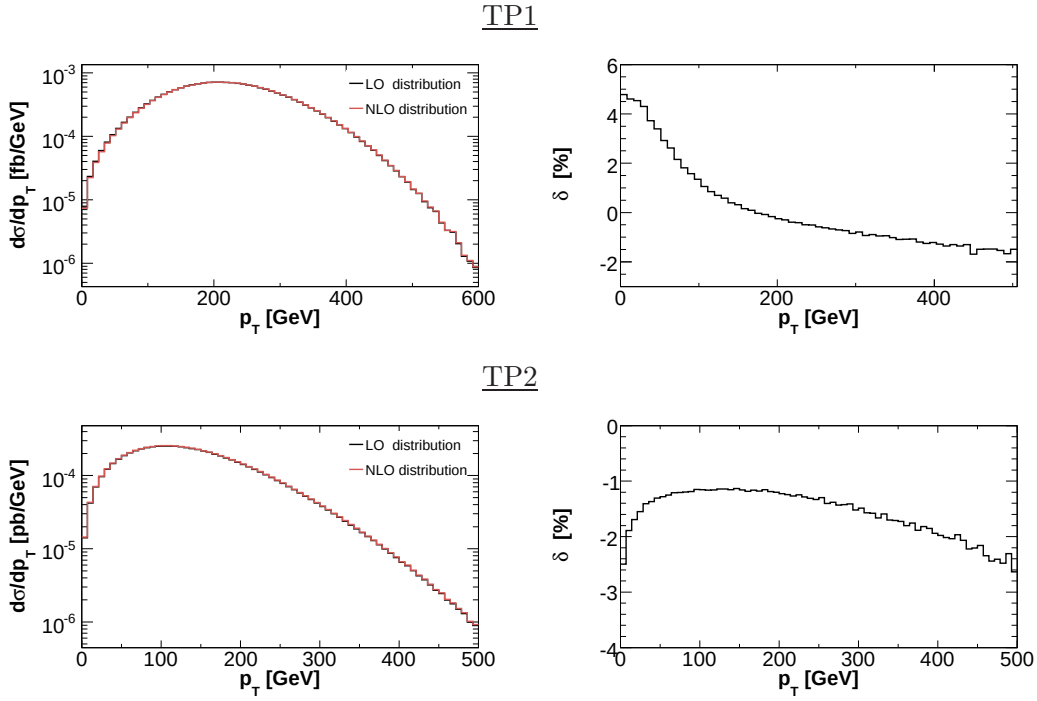

Figure 8. Same as figure 7, but considering the transverse momentum distribution.

Similar considerations hold in the case of the transverse momentum distribution, shown in figure 8. The shape of the distribution is not affected by the insertion of the electroweak corrections in both points. The electroweak corrections relative to the total contribution are of order of -2 to 4.5% in the case of the TP1 point and of the order of -2.5 to -1% in the TP2 scenario.

6 Conclusions

In this paper, we have computed the full $\mathcal{O}(\alpha_s^2\alpha)$ corrections to gluino pair production at the LHC and at the Tevatron. Two different renormalization schemes were used. The numerical value of the $\mathcal{O}(\alpha_s^2\alpha)$ contribution is rather independent on the renormalization scheme. The treatment of the IR and collinear singularities was performed within two different methods.

We have studied the numerical impact of the $\mathcal{O}(\alpha_s^2\alpha)$ contributions at the LHC in two different scenarios and we have performed scans over many regions of the parameter space. The EW corrections are negative and can be safely neglected. Compared to squark–anti-squark [25, 28] and squark-gluino [29] production, the EW contributions to gluino pair production are less important. The main reason is that the EW contributions do not enter the gluon fusion channel, which is the leading tree-level production channel in a wide part of the region of the parameter space investigated in this paper.

We have also provided numerical results for gluino pair production at the Tevatron selecting two scenarios belonging to the region of the parameter space investigated by the D0 and CDF collaborations. Again, the $\mathcal{O}(\alpha_s^2\alpha)$ contributions are small and negligible.

JHEP12(2009)012

Acknowledgments

We are indebted to Jan Germer, Wolfgang Hollik, and Maike Trenkel for useful discussions and for reading the manuscript. Michael Rauch is gratefully acknowledged for countless suggestions in the early stages of this work.

A Feynman diagrams

In this appendix we collect the relevant Feynman diagrams. In the following the label S (S^0) is used to denote charged (neutral) Higgs bosons. Moreover $V^0 = \gamma, Z$.

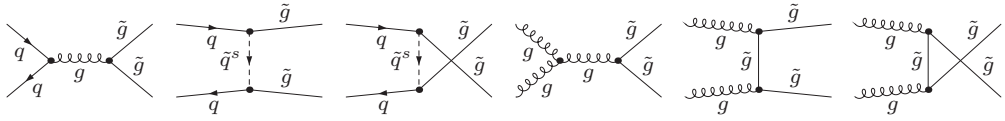

Figure 9. Tree-level diagrams for the processes $q\overline{q} \to \tilde{g}\tilde{g}$ and $gg \to \tilde{g}\tilde{g}$.

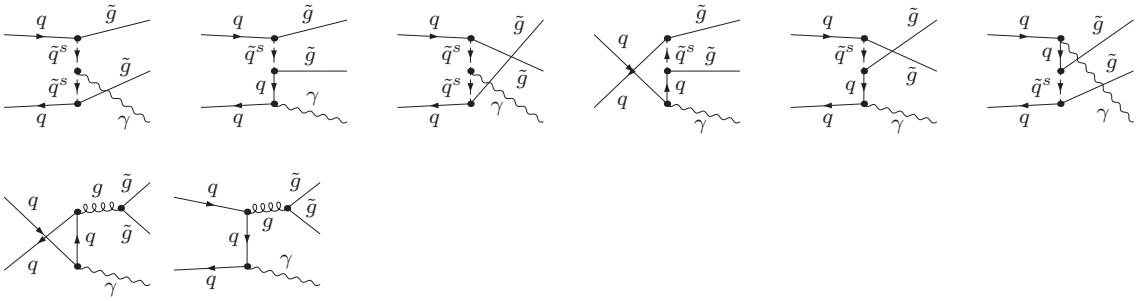

Figure 10. Tree-level diagrams for the real photon emission process $q\overline{q} \to \tilde{g}\tilde{g}\gamma$.

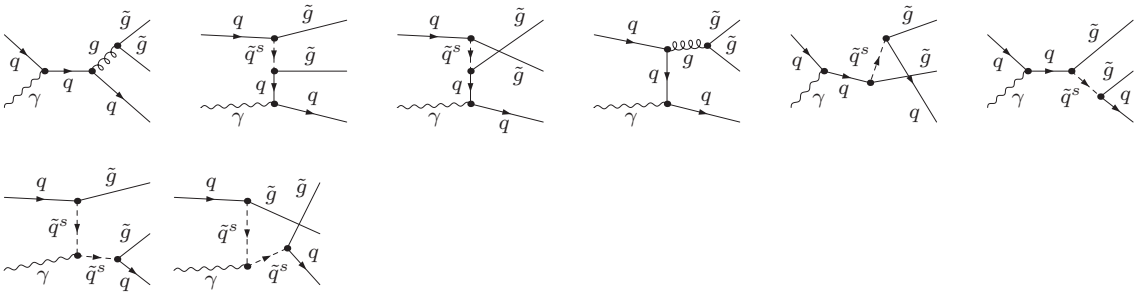

Figure 11. Tree-level diagrams for the process $q\gamma \to \tilde{g}\tilde{g}q$. The diagrams for the process $\gamma\overline{q} \to \tilde{g}\tilde{g}\overline{q}$ can be obtained inverting the arrows.

JHEP12(2009)012

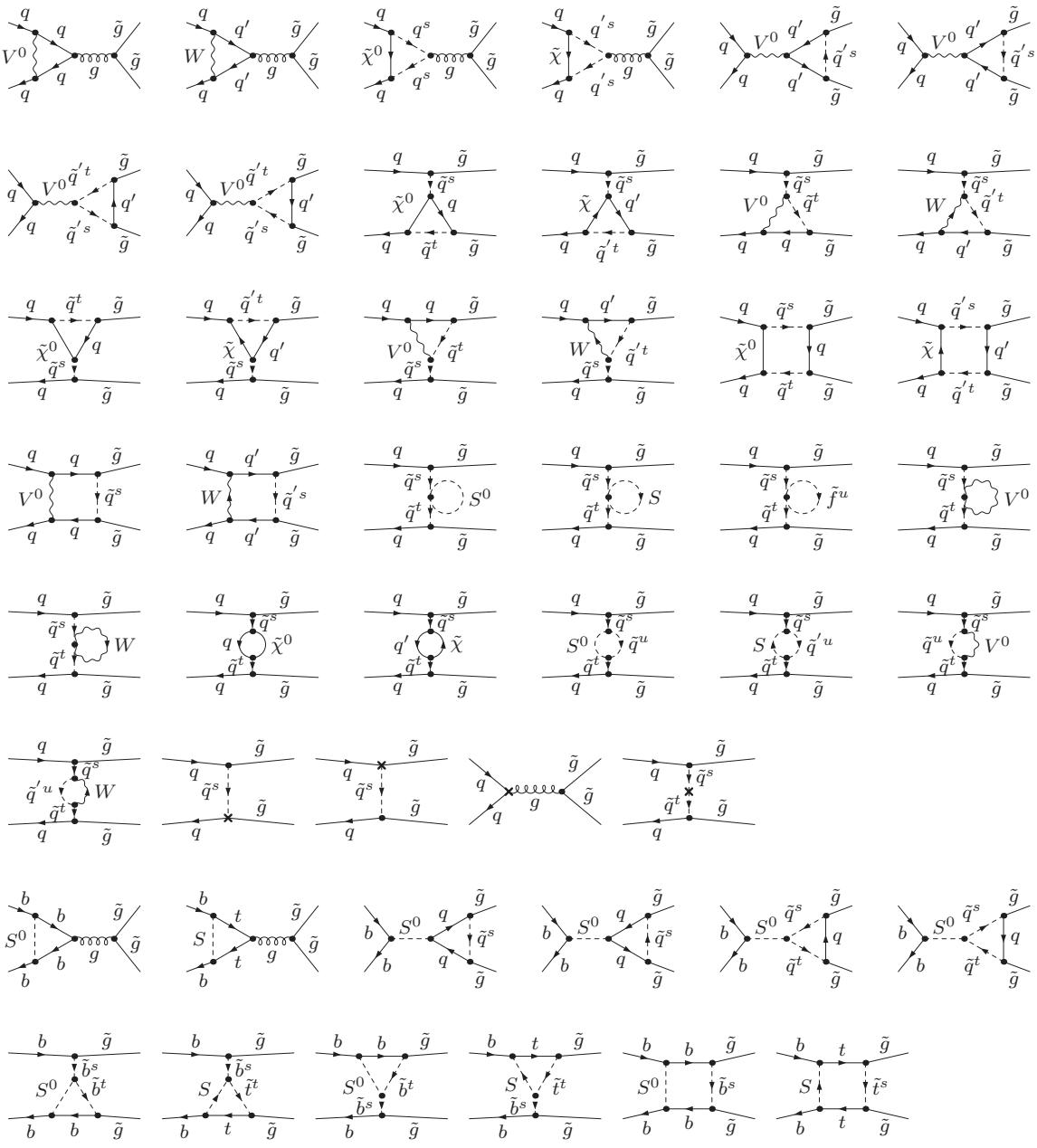

Figure 12. One-loop EW diagrams for the process $q\overline{q} \to \tilde{g}\tilde{g}$. Diagrams with crossed final states are not shown.

JHEP12(2009)012

Parameters		SPS1a′	SPS2	TP1	TP2
$\overline{\text{DR}}$ parameters evaluated at the scale $\mu_F = \mu_R = m_{\tilde{g}}$:					
	$\tan\beta$	10	10	3	3
	M_1 (GeV)	103	125	82	48
	M_2 (GeV)	193	232	153	91
	μ (GeV)	396	403	-318	-323
	A_b (GeV)	-945	-806	-580	-362
	A_τ (GeV)	-446	-181	-127	-77
On-shell masses (GeV):					
	m_{A^0}	426	1494	386	628
	$m_{\tilde{g}}$	608	784	499	337
	$m_{\tilde{u},L}$, $m_{\tilde{c},L}$	565	1562	475	562
	$m_{\tilde{u},R}$, $m_{\tilde{c},R}$	548	1557	463	561
	$m_{\tilde{d},R}$, $m_{\tilde{s},R}$	547	1557	463	562
	$m_{\tilde{t},1}$	586	1306	485	492
	$m_{\tilde{t},2}$	366	971	371	365
	$m_{\tilde{b},2}$	546	1545	463	562
	$m_{\tilde{\nu}_e}$, $m_{\tilde{\nu}_\mu}$	173	1456	179	500
	$m_{\tilde{e},R}$, $m_{\tilde{\mu},R}$	125	1453	155	503
	$m_{\tilde{\nu}_\tau}$	171	1450	179	500
	$m_{\tilde{\tau},1}$	195	1453	193	506
Mixing angle, stop sector:					
	$\cos\theta_{\tilde{t}}$	0.823	0.993	0.874	0.987

Table 5. Low-energy input parameters for the four SUSY scenarios considered, more details can be found in the text.

JHEP12(2009)012

B Input parameters

For the four SUSY scenarios considered in this work we use the set of low-energy input parameters introduced in table 5. Squarks belonging to the third generation have been labelled according to the conventions of ref. [38]. Since light quark masses are neglected, same-charge and same-chirality squarks of the first two generations are mass degenerate. The angle describing the mixing in the stop sector, $\tilde{\theta}_{\tilde{t}}$, is fixed as in ref. [38].

References

[1] J. Wess and B. Zumino, *Supergauge Transformations in Four-Dimensions*, *Nucl. Phys.* **B 70** (1974) 39 [SPIRES].

[2] D.V. Volkov and V.P. Akulov, *Is the Neutrino a Goldstone Particle?*, *Phys. Lett.* **B46** (1973) 109.

[3] H.P. Nilles, *Supersymmetry, Supergravity and Particle Physics*, *Phys. Rept.* **110** (1984) 1 [SPIRES].

[4] H.E. Haber and G.L. Kane, *The Search for Supersymmetry: Probing Physics Beyond the Standard Model*, *Phys. Rept.* **117** (1985) 75 [SPIRES].

[5] R. Barbieri, *Looking Beyond the Standard Model: The Supersymmetric Option*, *Riv. Nuovo Cim.* **11N4** (1988) 1.

[6] J.R. Ellis, S. Heinemeyer, K.A. Olive, A.M. Weber and G. Weiglein, *The Supersymmetric Parameter Space in Light of B^- physics Observables and Electroweak Precision Data*, *JHEP* **08** (2007) 083 [arXiv:0706.0652] [SPIRES].

[7] O. Buchmueller et al., *Prediction for the Lightest Higgs Boson Mass in the CMSSM using Indirect Experimental Constraints*, *Phys. Lett.* **B 657** (2007) 87 [arXiv:0707.3447] [SPIRES].

[8] Muon g-2 collaboration, G.W. Bennett et al., *Measurement of the Positive Muon Anomalous Magnetic Moment to 0.7 ppm*, *Phys. Rev. Lett.* **89** (2002) 101804 [hep-ex/0208001] [SPIRES].

[9] Muon g-2 collaboration, G.W. Bennett et al., *Measurement of the negative muon anomalous magnetic moment to 0.7 ppm*, *Phys. Rev. Lett.* **92** (2004) 161802 [hep-ex/0401008] [SPIRES].

[10] ATLAS collaboration, G. Aad et al., *Expected Performance of the ATLAS Experiment. Detector, Trigger and Physics*, arXiv:0901.0512 [SPIRES].

[11] CMS collaboration, G.L. Bayatian et al., *CMS technical design report, volume II: Physics performance*, *J. Phys.* **G 34** (2007) 995 [SPIRES].

[12] A. Alves, O. Eboli and T. Plehn, *It's a gluino*, *Phys. Rev.* **D 74** (2006) 095010 [hep-ph/0605067] [SPIRES].

[13] R.M. Barnett, J.F. Gunion and H.E. Haber, *Discovering supersymmetry with like sign dileptons*, *Phys. Lett.* **B 315** (1993) 349 [hep-ph/9306204] [SPIRES].

[14] S. Kraml and A.R. Raklev, *Same-sign top quarks as signature of light stops at the LHC*, *Phys. Rev.* **D 73** (2006) 075002 [hep-ph/0512284] [SPIRES].

[15] S.Y. Choi, M. Drees, A. Freitas and P.M. Zerwas, *Testing the Majorana Nature of Gluinos and Neutralinos*, *Phys. Rev.* **D 78** (2008) 095007 [arXiv:0808.2410] [SPIRES].

[16] M.M. Nojiri et al., *Physics Beyond the Standard Model: Supersymmetry*, arXiv:0802.3672 [SPIRES].

[17] G.L. Kane and J.P. Leveille, *Experimental Constraints on Gluino Masses and Supersymmetric Theories*, *Phys. Lett.* **B 112** (1982) 227 [SPIRES].

[18] P.R. Harrison and C.H. Llewellyn Smith, *Hadroproduction of Supersymmetric Particles*, *Nucl. Phys.* **B 213** (1983) 223 [SPIRES].

[19] E. Reya and D.P. Roy, *Supersymmetric particle production at $p\bar{p}$ collider energies*, *Phys. Rev.* **D 32** (1985) 645 [SPIRES].

[20] S. Dawson, E. Eichten and C. Quigg, *Search for Supersymmetric Particles in Hadron-Hadron Collisions*, *Phys. Rev.* **D 31** (1985) 1581 [SPIRES].

JHEP12(2009)012

[21] W. Beenakker, R. Hopker, M. Spira and P.M. Zerwas, *Squark and gluino production at hadron colliders*, *Nucl. Phys.* **B 492** (1997) 51 [hep-ph/9610490] [SPIRES].

[22] W. Beenakker, R. Hopker and M. Spira, *PROSPINO: A program for the Production of Supersymmetric Particles In Next-to-leading Order QCD*, hep-ph/9611232 [SPIRES].

[23] A. Kulesza and L. Motyka, *Threshold resummation for squark-antisquark and gluino- pair production at the LHC*, *Phys. Rev. Lett.* **102** (2009) 111802 [arXiv:0807.2405] [SPIRES].

[24] A. Kulesza and L. Motyka, *Soft gluon resummation for the production of gluino-gluino and squark-antisquark pairs at the LHC*, *Phys. Rev.* **D 80** (2009) 095004 [arXiv:0905.4749] [SPIRES].

[25] W. Hollik, M. Kollar and M.K. Trenkel, *Hadronic production of top-squark pairs with electroweak NLO contributions*, *JHEP* **02** (2008) 018 [arXiv:0712.0287] [SPIRES].

[26] M. Beccaria, G. Macorini, L. Panizzi, F.M. Renard and C. Verzegnassi, *Stop-antistop and sbottom-antisbottom production at LHC: a one-loop search for model parameters dependence*, *Int. J. Mod. Phys.* **A 23** (2008) 4779 [arXiv:0804.1252] [SPIRES].

[27] S. Bornhauser, M. Drees, H.K. Dreiner and J.S. Kim, *Electroweak Contributions to Squark Pair Production at the LHC*, *Phys. Rev.* **D 76** (2007) 095020 [arXiv:0709.2544] [SPIRES].

[28] W. Hollik and E. Mirabella, *Squark anti-squark pair production at the LHC: the electroweak contribution*, *JHEP* **12** (2008) 087 [arXiv:0806.1433] [SPIRES].

[29] W. Hollik, E. Mirabella and M.K. Trenkel, *Electroweak contributions to squark-gluino production at the LHC*, *JHEP* **02** (2009) 002 [arXiv:0810.1044] [SPIRES].

[30] T. Hahn, *Generating Feynman diagrams and amplitudes with FeynArts 3*, *Comput. Phys. Commun.* **140** (2001) 418 [hep-ph/0012260] [SPIRES].

[31] T. Hahn and C. Schappacher, *The implementation of the minimal supersymmetric standard model in FeynArts and FormCalc*, *Comput. Phys. Commun.* **143** (2002) 54 [hep-ph/0105349] [SPIRES].

[32] T. Hahn and M. Pérez-Victoria, *Automatized one-loop calculations in four and D dimensions*, *Comput. Phys. Commun.* **118** (1999) 153 [hep-ph/9807565] [SPIRES].

[33] T. Hahn and M. Rauch, *News from FormCalc and LoopTools*, *Nucl. Phys. Proc. Suppl.* **157** (2006) 236 [hep-ph/0601248] [SPIRES].

[34] H. Eberl, M. Kincel, W. Majerotto and Y. Yamada, *One-loop corrections to the chargino and neutralino mass matrices in the on-shell scheme*, *Phys. Rev.* **D 64** (2001) 115013 [hep-ph/0104109] [SPIRES].

[35] A. Brignole, G. Degrassi, P. Slavich and F. Zwirner, *On the two-loop sbottom corrections to the neutral Higgs boson masses in the MSSM*, *Nucl. Phys.* **B 643** (2002) 79 [hep-ph/0206101] [SPIRES].

[36] W. Oller, H. Eberl, W. Majerotto and C. Weber, *Analysis of the chargino and neutralino mass parameters at one-loop level*, *Eur. Phys. J.* **C 29** (2003) 563 [hep-ph/0304006] [SPIRES].

[37] W. Hollik and H. Rzehak, *The sfermion mass spectrum of the MSSM at the one-loop level*, *Eur. Phys. J.* **C 32** (2003) 127 [hep-ph/0305328] [SPIRES].

[38] S. Heinemeyer, W. Hollik, H. Rzehak and G. Weiglein, *High-precision predictions for the MSSM Higgs sector at $O(\alpha_b\alpha_s)$*, *Eur. Phys. J.* **C 39** (2005) 465 [hep-ph/0411114] [SPIRES].

JHEP12(2009)012

[39] T. Banks, *Supersymmetry and the Quark Mass Matrix*, *Nucl. Phys.* **B 303** (1988) 172 [SPIRES].

[40] L.J. Hall, R. Rattazzi and U. Sarid, *The Top quark mass in supersymmetric SO(10) unification*, *Phys. Rev.* **D 50** (1994) 7048 [hep-ph/9306309] [SPIRES].

[41] R. Hempfling, *Yukawa coupling unification with supersymmetric threshold corrections*, *Phys. Rev.* **D 49** (1994) 6168 [SPIRES].

[42] M.S. Carena, M. Olechowski, S. Pokorski and C.E.M. Wagner, *Electroweak symmetry breaking and bottom-top Yukawa unification*, *Nucl. Phys.* **B 426** (1994) 269 [hep-ph/9402253] [SPIRES].

[43] M.S. Carena, D. Garcia, U. Nierste and C.E.M. Wagner, *Effective Lagrangian for the $\bar{t}bH^+$ interaction in the MSSM and charged Higgs phenomenology*, *Nucl. Phys.* **B 577** (2000) 88 [hep-ph/9912516] [SPIRES].

[44] H. Eberl, K. Hidaka, S. Kraml, W. Majerotto and Y. Yamada, *Improved SUSY QCD corrections to Higgs boson decays into quarks and squarks*, *Phys. Rev.* **D 62** (2000) 055006 [hep-ph/9912463] [SPIRES].

[45] V.N. Baier, V.S. Fadin and V.A. Khoze, *Quasireal electron method in high-energy quantum electrodynamics*, *Nucl. Phys.* **B65** (1973) 381.

[46] A. Denner, *Techniques for calculation of electroweak radiative corrections at the one loop level and results for W physics at LEP-200*, *Fortschr. Phys.* **41** (1993) 307 [arXiv:0709.1075] [SPIRES].

[47] W. Hollik, T. Kasprzik and B.A. Kniehl, *Electroweak corrections to W-boson hadroproduction at finite transverse momentum*, *Nucl. Phys.* **B 790** (2008) 138 [arXiv:0707.2553] [SPIRES].

[48] S. Dittmaier, *A general approach to photon radiation off fermions*, *Nucl. Phys.* **B 565** (2000) 69 [hep-ph/9904440] [SPIRES].

[49] S. Dittmaier, A. Kabelschacht and T. Kasprzik, *Polarized QED splittings of massive fermions and dipole subtraction for non-collinear-safe observables*, *Nucl. Phys.* **B 800** (2008) 146 [arXiv:0802.1405] [SPIRES].

[50] K.P.O. Diener, S. Dittmaier and W. Hollik, *Electroweak higher-order effects and theoretical uncertainties in deep-inelastic neutrino scattering*, *Phys. Rev.* **D 72** (2005) 093002 [hep-ph/0509084] [SPIRES].

[51] A.D. Martin, R.G. Roberts, W.J. Stirling and R.S. Thorne, *Parton distributions incorporating QED contributions*, *Eur. Phys. J.* **C 39** (2005) 155 [hep-ph/0411040] [SPIRES].

[52] Particle Data Group collaboration, W.M. Yao et al., *Review of particle physics*, *J. Phys.* **G 33** (2006) 1 [SPIRES].

[53] J.A. Aguilar-Saavedra et al., *Supersymmetry parameter analysis: SPA convention and project*, *Eur. Phys. J.* **C 46** (2006) 43 [hep-ph/0511344] [SPIRES].

[54] B.C. Allanach et al., *The Snowmass points and slopes: Benchmarks for SUSY searches*, *Eur. Phys. J.* **C 25** (2002) 113 [hep-ph/0202233] [SPIRES].

[55] W. Porod, *SPheno, a program for calculating supersymmetric spectra, SUSY particle decays and SUSY particle production at e^+e^- colliders*, *Comput. Phys. Commun.* **153** (2003) 275 [hep-ph/0301101] [SPIRES].

JHEP12(2009)012

[56] E. Accomando, A. Denner and C. Meier, *Electroweak corrections to $W\gamma$ and $Z\gamma$ production at the LHC*, *Eur. Phys. J.* **C 47** (2006) 125 [hep-ph/0509234] [SPIRES].

[57] ALEPH collaboration, S. Schael et al., *Search for neutral MSSM Higgs bosons at LEP*, *Eur. Phys. J.* **C 47** (2006) 547 [hep-ex/0602042] [SPIRES].

[58] D0 collaboration, V.M. Abazov et al., *Search for squarks and gluinos in events with jets and missing transverse energy in $p\bar{p}$ collisions at $\sqrt{s} = 1.96$ TeV*, *Phys. Lett.* **B 638** (2006) 119 [hep-ex/0604029] [SPIRES].

[59] S. Heinemeyer, W. Hollik and G. Weiglein, *FeynHiggs: a program for the calculation of the masses of the neutral CP-even Higgs bosons in the MSSM*, *Comput. Phys. Commun.* **124** (2000) 76 [hep-ph/9812320] [SPIRES].

[60] M. Frank et al., *The Higgs boson masses and mixings of the complex MSSM in the Feynman-diagrammatic approach*, *JHEP* **02** (2007) 047 [hep-ph/0611326] [SPIRES].

[61] G. Degrassi, S. Heinemeyer, W. Hollik, P. Slavich and G. Weiglein, *Towards high-precision predictions for the MSSM Higgs sector*, *Eur. Phys. J.* **C 28** (2003) 133 [hep-ph/0212020] [SPIRES].

[62] D0 collaboration, B. Abbott et al., *Search for squarks and gluinos in events containing jets and a large imbalance in transverse energy*, *Phys. Rev. Lett.* **83** (1999) 4937 [hep-ex/9902013] [SPIRES].

[63] CDF collaboration, A.A. Affolder et al., *Search for gluinos and scalar quarks in $p\bar{p}$ collisions at $\sqrt{s} = 1.8$ TeV using the missing energy plus multijets signature*, *Phys. Rev. Lett.* **88** (2002) 041801 [hep-ex/0106001] [SPIRES].

[64] D0 collaboration, V.M. Abazov et al., *Search for squarks and gluinos in events with jets and missing transverse energy using 2.1 fb^{-1} of $p\bar{p}$ collision data at $\sqrt{s} = 1.96$ TeV*, *Phys. Lett.* **B 660** (2008) 449 [arXiv:0712.3805] [SPIRES].

JHEP12(2009)012